frontiers | Frontiers in Earth Science

TYPE Original Research
PUBLISHED 09 January 2024
DOI 10.3389/feart.2023.1284151

OPEN ACCESS

EDITED BY
Guillermo Booth-Rea,
University of Granada, Spain

REVIEWED BY
Laura Gómez de la Peña,
Institue of Marine Sciences (ICM-CSIC), Spain
Simona Todaro,
University of Palermo, Italy

*CORRESPONDENCE
Rafael André Belotto Plawiak,
rplawiak@id.uff.br

†PRESENT ADDRESSES
Rafael André Belotto Plawiak, Laboratory of Sedimentary Geology, Institute of Geosciences, Federal University of Rio de Janeiro, Rio de Janeiro, Brazil

RECEIVED 28 August 2023
ACCEPTED 29 November 2023
PUBLISHED 09 January 2024

CITATION
Plawiak RAB, Carvalho MJ, Sombra CL, Brandão DR, Mepen M, Ferrari AL and Gambôa LAP (2024), Structural controls of the migration of mantle-derived CO_2 offshore in the Santos Basin (Southeastern Brazil).
Front. Earth Sci. 11:1284151.
doi: 10.3389/feart.2023.1284151

Structural controls of the migration of mantle-derived CO_2 offshore in the Santos Basin (Southeastern Brazil)

Rafael André Belotto Plawiak[1]*†, Marcelo José Carvalho[1], Cristiano Leite Sombra[1], Davy Raeder Brandão[1], Michelle Mepen[2], André Luiz Ferrari[1] and Luiz Antônio Pierantoni Gambôa[1]

[1]Laboratory of Marine Geology, Institute of Geosciences, Fluminense Federal University, Niterói, Brazil, [2]Petrogal Brasil S.A, Rio de Janeiro, Brazil

We present a multi-scale conceptual model based on structural controls of the migration of mantle-derived CO_2 offshore in the Santos Basin (Southeastern Brazil). We assembled the model from a regional 2D seismic reflection line integrated with potential gravimetric field data and a local 3D seismic reflection volume integrated with well data (lithologies and *in situ* stress). (i) The geochemical isotope range of $\delta^{13}C_{CO2}$ falls mostly within −7‰ and −5‰ and shows relatively high values for $^3He/^4He$ represented by an R/Ra rate of up to 5.60, indicating CO_2 mantle generation and degassing. (ii) Seismic interpretation feasibly validated by potential gravimetric responses of the crustal structure (Moho discontinuity) show CO_2 migration through deep-seated faults in a region of highly stretched continental crust with oceanward mantle uprising. (iii) Early Cretaceous basement highs generated in an obliquely syn-rift faulting system control CO_2 accumulation in thermogenic travertines (hydrothermal carbonate reservoirs of continental lakes), and Aptian evaporites subsequently trap it.

KEYWORDS

structural controls, mantle-derived carbon dioxide, oblique syn-rift structures, thermogenic travertines, pre-salt Santos Basin, multi-scale conceptual model

1 Introduction

Mantle-derived CO_2 occurrences have been well documented in different geological contexts around the world by various researchers (Lowenstern, 2001; Chiodini et al., 2004; Bigi et al., 2014; Hutchison et al., 2015; Lee et al., 2016; Lee et al., 2019; Yang et al., 2021; Hill et al., 2022; Xia et al., 2022). In the Songliao Basin (China), Liu et al. (2018) reported that CO_2 mainly comes from deep magma, and accumulates mostly in the mantle uplift areas with the development of basement faults or strong deep hydrothermal activity. They also observed that this gas migrates mainly through the large-scale, low angle basin-controlling basement faults. Miao et al. (2020) found that in the Bohai Basin (NE China), the lithosphere scale strike–slip faults are the main conduits for the migration of CO_2 below the middle crust. Chiodini et al. (2004) suggested that in a non-volcanic area in the central Apennines (Italy), this gas originates from a deep, mantle-related source, and that extensional tectonics and seismic activity influence its migration. Della Porta (2015) showed that in Central Italy, fault activity affects the development of hydrologically closed lacustrine basins, groundwater flow,

and the location of hydrothermal vents, and classified their deposits as thermogenic travertines with thermally generated CO_2 of magmatic mantle-derived origin.

Xia et al. (2022) stated that, typically, significant quantities of CO_2 originate from three sources in the subsurface: organic matter maturation, magma degassing, and decomposition of carbonate minerals. Santos Neto et al. (2012) interpreted that up to 80% of CO_2 anomalies in the Santos Basin are mantle-derived due to the isotope range of $\delta^{13}C_{CO2}$ being mostly within −7‰ and −5‰ and the relatively high values for $^3He/^4He$, represented by an R/Ra rate of up to 5.60. Gambôa et al. (2019) and Ferraz et al. (2019) proposed, based on magnetic and gravimetric regional data, that deep faults could possibly be the way for migration of this gas to the pre-salt hydrocarbon reservoirs in areas like Jupiter, where highly stretched continental crust and magmatic intrusions may have connected with mantle CO_2 degassing. Ysaccis et al. (2019) speculated that deep-seated faults of the Jupiter structure could explain the occurrence of the high CO_2 content found in this oil/gas prospect.

The Jupiter exploratory wells in the Central Santos Basin reached up 77% mean CO_2 values. Besides Jupiter, other areas of the basin have stated high CO_2 contents (Figure 1) (Freitas et al., 2022) and their production have faced several risks, such as production facilities (Beltrão et al., 2009) and corrosion of flow lines and production columns (Beltrão et al., 2009; Freitas et al., 2022).

We present structural evidence of a mantle-derived CO_2 migration in the Jupiter area based on: (i) 2D/3D seismic reflection data; (ii) potential gravimetric field (Bouguer and residual anomaly); and (iii) *in situ* stress analysis and lithologies from wells. Our goal is to propose a conceptual model for CO_2 migration in a mantle uplifted, highly stretched continental crust area, where deep-seated faults act as conduits connecting to the syn-rift basement faults, creating buildups with thermogenic travertines through the pre-salt section, from hydrothermal fluids that might be responsible for CO_2 anomalous values in Jupiter area. This study provides critical information on understanding the mantle-derived CO_2 migration offshore in the Santos Basin.

2 Tectonic setting

The Early Cretaceous giant rift Santos Basin is located along the South Atlantic Brazilian margin with a width of approximately 700 km and 300 km of extension (Baptista et al., 2023). It is an asymmetrical basin that lies on a prominent irregular marginal plateau in the Southeastern Brazilian continental margin, the São Paulo Plateau. Intruding diapiric structures that have disturbed the overlying sediments mainly created the plateau (Kumar et al., 1977). The sedimentary history of the Santos Basin and the São Paulo Plateau suggests that the two regions have been structurally continuous, at least since the Late Cretaceous. The region occupied by the plateau has acted as a depocenter and has evolved as a marginal plateau since the termination of evaporitic deposition in the South Atlantic (Kumar and Gambôa, 1979). The Jupiter area lies in a region of highly stretched continental crust on the São Paulo Plateau, described as the Outer Hingeline, on the edge of the Santos Outer High (Gomes et al., 2009). A synthetic system of NNE-WSW faults, structurally uplifted by rotation of fault blocks in domino style (Plawiak et al., 2022), dominates the Jupiter's structure.

Neoproterozoic-Cambrian metamorphic rocks from the NE-SW Ribeira Orogenic Belt compose the basement of Santos Basin (Heilbron et al., 2008). The Gondwana Supercontinent started to break up in the Early Cretaceous, and intense basaltic volcanism occurred due to early stretching of the crust, developing the rift phase between South America and Africa in the Hauterivian (Moreira et al., 2007). The South Atlantic margin inherited a NE-SW orientation from Late Proterozoic structures, and the syn-rift architecture resulted in an oblique orientation to the margin (Meisling et al., 2001). The NE-SW inheritance associated

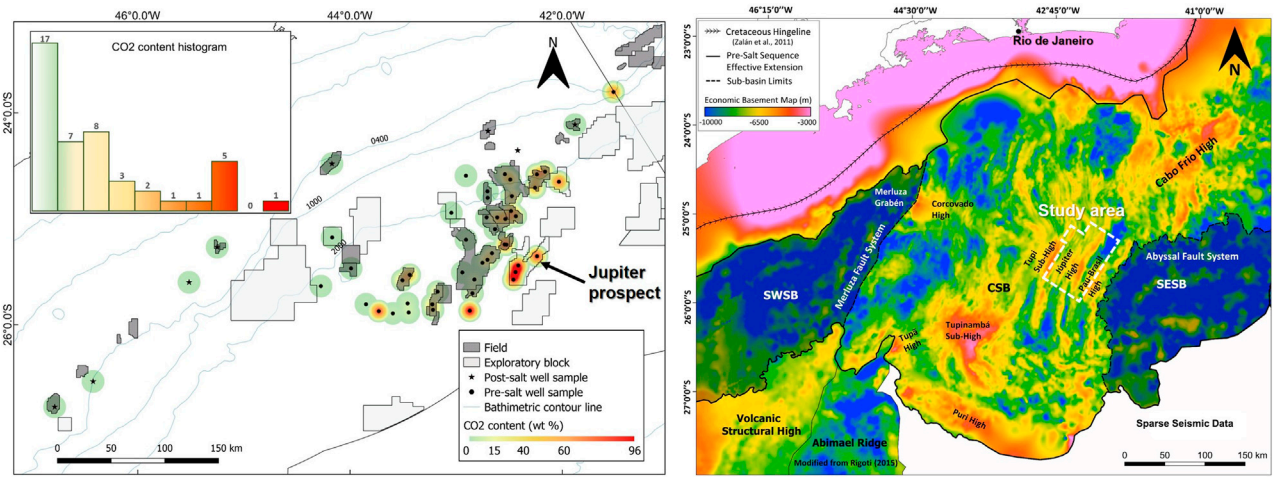

FIGURE 1
To the left, heat map of CO_2 in the Santos Basin and the location of the Jupiter prospect showing high CO_2 content (77% wt mean value). To the right, study area location in the Central Santos Basin (CSB) corresponding to the 3D seismic survey in Jupiter. Both maps adapted with permission from Elsevier by Freitas et al. (2022), licensed for reuse under reference number 5681941283432.

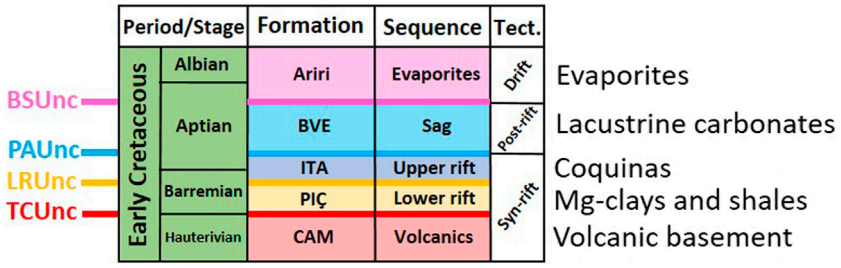

FIGURE 2
Simplified stratigraphic chart of the pre-salt sequences in the Santos Basin (after Moreira et al., 2007). Lithostratigraphic sequences separated by unconformities (Unc): TCUnc-Top Camboriú, LRUnc-Top Lower Rift, PAUnc-Pre-Alagoas and BSUnc-Base Salt. Formations: Camboriú-CAM, Piçarras-PIÇ, Itapema-ITA, Barra Velha-BVE and Ariri. Tectonic events (Tect.).

with a WSW-ENE rift extension created segmented faults with sinuous rombo-shaped and left-lateral *en échelon* patterns, as observed in the Jupiter rift shoulder (Plawiak et al., 2022) and in the East African Rift System (Zwaan and Schreurs, 2017), and also modeled in the Central Santos Basin (Pereira et al., 2021). Syn-rift structures have been reactivated at least three times in the South Atlantic Margin, in the Late Cretaceous, Eocene, and Miocene (Zalán and Oliveira, 2005; Fetter, 2009; Cobbold et al., 2010), with important consequences for hydrothermal vent formations (Magee et al., 2016). A late-rift left-lateral transtensional NE-SW shear zone (Late-Aptian to Early Albian) affected the syn-rift structures ("Helmut" Shear Zone—HSZ, Dehler et al., 2016).

We can divide the syn-rift sequence into three lithostratigraphic units, separated by unconformities (Moreira et al., 2007). The first unit represents rift onset on the volcanic rocks of the Camboriú Formation (CAM), marked by the Top Camboriú Unconformity (TCUnc) in 130 M.y. The second unit, lower rift, is composed of the Mg-clays and talcostevensitic ooliths of the Piçarras Formation (PIÇ), marked at the top by Lower Rift Unconformity (LRUnc) in 126 M.y. The third, upper rift, is composed of the bioclastic carbonates (coquinas) and siltic-clay intercalations of the Itapema Formation (ITA), marked at the top by the Pre-Alagoas Unconformity (PAUnc) in 123 M.y. (Figure 2).

The post-rift sequence represents the SAG phase (Moreira et al., 2007), Barra Velha Formation (BVE), with lacustrine continental carbonate deposits, and rudstones with fragments of volcanic rocks. Locally, carbonates can be dolomitized or silicified. The deposition of laminitic and spherulitic clay carbonates marks the Intra-Alagoas Unconformity (IAUnc) in 117 M.y. The deposition of the evaporites of the Ariri Formation marks the Base Salt Unconformity (BSUnc) in 113 M.y. and represents the passage to the continental break up—drift—phase (Moreira et al., 2007) (Figure 2).

We can divide the magmatism in the Santos Basin into two groups: Lower Cretaceous and Upper Cretaceous/Paleogen (De Luca et al., 2015). The former is usually associated with the rift phase with basalt-tholeiitic magmas that showed Ar-Ar ages between 137–122 M.y. The second group is usually associated with alkaline series, represented by ultramafic, mafic (basaltic), and felsic magmas (trachytes/syenites, phonolites/nepheline syenites) with Ar-Ar ages between 90–43 M.y. (De Luca et al., 2015).

Plawiak et al. (2022) have identified late-rift/post-rift fault-related structures and km-scale elongated conical-shaped buildups forming fissure ridges genetically related to the syn-rift basement faults in the Jupiter area. The fault-related features highlighted by Plawiak et al. (2022) are widespread in the Jupiter area and its spatial and temporal distribution may indicate fault reactivations responsible for fluid migration at depth, especially mantle-derived CO_2.

Sombra et al. (2023) conducted a study at the Iara Complex in the Santos Basin that demonstrated that syn-rift faults act as pathways for hydrothermal fluids that precipitate as carbonate buildups. Mounded features are frequently above faults and structural highs. Considering the moderate to high CO_2 content in pre-salt reservoirs, this relationship suggests that degassing of upwards migrating fluids rich in CO_2, shifting pH towards more alkaline values, may have played an important role in calcite precipitation and mounds growth above faults (Sombra et al., 2023).

ION-GXT acquired 2D wide-angle reflection seismic profiles across the Santos Basin-São Paulo Plateau System (SSPS) in 2010/2011. Several interpretations have been presented to better understand the mantle-crust relationships and its inheritance influence on the tectonostratigraphic evolution of the Santos Basin syn-rift sequences (Zalán et al., 2011; Kumar et al., 2012; Evain et al., 2015; Rigoti, 2015; Dehler et al., 2016; Araujo et al., 2022). There is a consensus among these authors that the continental crust is highly stretched under the Jupiter structure.

3 Data and methods

We used the Jupiter 3D Post Stack Depth Migrated (PSDM) seismic reflection volume to interpret the top volcanic basement and syn-rift faults. The seismic area was 4,270 m^2 and acquisition geometry settings had the following parameters: group interval of 12.5 m, recording sample rate of 2 ms, and shot point's interval of 25 m with streamer depth of 9 m. We used the Kirchhoff algorithm for time-depth PSDM migration: (i) velocity input grid of 25 m × 25 m × 10 m with a sample rate of 6 ms; (ii) output grid of 50 m × 50 m with an offset range between 375-8,075 m.

We used an ultra-deep 2D PSDM seismic reflection line (ION-GXT, Brasil Span Project, line 0375, W-E oriented) to interpret

Moho discontinuity, top volcanic basement, base/top of evaporites and sea bottom horizons. We used the gravity Bouguer profile (from this work) to support seismic interpretations at deeper depths. We checked the wide-angle refraction profiles from Evain et al. (2015) as references for Moho interpretations. The maximum seismic depth was 40 km. The seismic length was 820 km and acquisition geometry settings had the following parameters: group interval of 25 m, recording sample rate of 4 ms, and shot point's interval of 50 m with streamer average depth of 9.5 m. We used the Kirchhoff algorithm for time-depth PSDM migration: (i) record length of 25 km with an interval of 12.5 m; (ii) crustal velocities were derived from gravity analysis; (iii) the final velocity model including salt (4,575 m/s constant velocity) and sediment velocity grids (with manual and tomographic update) were merged with crustal velocities. Gravity analysis defined the following velocity layers: Upper Crust 5,770 m/s, Middle Crust 6,600 m/s, Lower Crust 7,180 m/s and Upper Mantle 8,190 m/s.

We used Decision Space® Geosciences (DSG) by Landmark for both 2D and 3D seismic interpretations. We generated the 3D volcanic basement grids using the Dynamic Framework to Fill™ workspace (in DSG) with the Refinement Gridding method, which applies a minimum curvature algorithm to regular grids. We generated a Semblance color scale (blue/black) within the Azimuth seismic attribute from DSG to highlight structural patterns in depth slices from the amplitude 3D volume.

We used the altimetric data from the GEBCO global database. The GEBCO project—General Bathymetric Chart of the Oceans (https://www.gebco.net/)—provides satellite altimetry data with a resolution of 15 arc seconds. We used the Free-Air anomaly data from the Topex/Poseidon project database (https://topex.ucsd.edu/cgi-bin/get_data.cgi) with a resolution of 2 arc minutes. We loaded, calculated, and interpreted all potential data with Geosoft software (Oasis Montaj® by Seequent).

We interpolated the altimetric and gravimetric data in regular meshes of 2 arc minutes, using the method of minimum curvature with adjustable tension (Smith and Wessel, 1990). We used 0.35 for the altimetric data and 0.25 for the gravimetric data as the tension values.

We calculated the Bouguer anomaly using Parker's method (Parker, 1973) which uses the Fourier transform to calculate the gravimetric anomaly between two media with distinct densities. The density formula used to calculate the Bouguer anomaly was:

$$\rho = \rho_{Crust} - \rho_{Water}$$

We used the density values of 2.67 g/cm^3 for the continental crust (Hinze, 2003) and 1.03 g/cm^3 for seawater.

We performed the separation between regional and residual gravimetric anomalies through spectral filtering (Nettleton, 1954). We determined the regional gravimetric field from a low-pass filter. We estimated the 500 km wavelength of the regional anomalies from the power spectrum graph of the Bouguer anomaly (Carvalho et al., 2022). We obtained the enhancement of the small wavelength anomalies (residual anomalies) by subtracting the large wavelength anomalies from the Bouguer map.

We analyzed and interpreted acoustic image logs with Decision Space Petrophysics software by Landmark in all the Jupiter wells (1-BRSA-559A-RJS, 3-BRSA-967A-RJS, 3-BRSA-1183-RJS, and 3-BRSA-1246-RJS). We interpreted breakout structures on Ultrasonic Borehole Images (UBI ©Schlumberger) logging for *in situ* stress analysis and estimation of the Maximum Horizontal Stress (SHmax) orientation azimuth. We achieved the quality-ranked stress data from the World Stress Map Project (WSM—Heidbach et al., 2010). The WSM quality ranking system ranges from A-quality (highest; stress orientation accurate to within ±15°) to E-quality (lowest; no reliable stress orientation) and provides an easy assessment of the accuracy, scale, and reliability of each stress indicator.

We checked cores and side-core description reports from the Brazilian Petroleum National Agency (ANP) for the identification of lithologies and structures on wells 3-BRSA-967A-RJS and 3-BRSA-1183-RJS (Costa et al., 2017).

4 Results and discussion

4.1 Seismic amplitude 3D volume

We observed clear segmentation of the syn-rift faults, showing rectilinear to sinuous patterns, with strike variation from N to NE (Figure 3A). We separated two structural domains based on two distinct structural styles: Northwest (NW) and Southeast (SE) (Figure 3B).

NW Domain—The faults have *en échelon* and rombo-shaped (sigmoidal) patterns in map sight, with relay ramps stepping the faults' segments (Figure 3B). In section view, structural styles include extensional planar to curved rotational fault blocks (domino structural style), forming hemi-grabens with mean dips 30° (Figure 4).

SE Domain—The faults show rectilinear to curved patterns that are less segmented than the NW Domain in map sight (Figure 3B). In section view, structural styles include negative flower-like structures with synthetic faults mean dips of 35° and antithetic mean dips of 55° (Figure 4). Depocenter thicknesses reach up to 5 km, salt welds occur in the southernmost corner of the study area, and top volcanic basement deeper depths are approximately 11 km.

The arrows in the dip sections of Figure 4 highlight the fault-related structures clearly connected to the structural highs and fault tip propagations. Conical-shaped buildups in section view (blue arrows in Figure 4) and km-scale fissure ridges in map sight (Figure 3B). The syn-rift basement faults may be genetically related to these structures. Volcanic-like cones and chimneys, also folding and cutting some layers above fault tips, occur between the top volcanic basement and the base of salt (yellow arrows in Figure 4). The volcanic-like cones and chimneys, identified as late-rift/post-rift fault-related structures by Plawiak et al. (2022), could correlate with at least one of the three events of reactivation of syn-rift structures observed in the South Atlantic Margin: Late Cretaceous, Eocene, and Miocene (Zalán and Oliveira, 2005; Fetter, 2009; Cobbold et al., 2010. Alternatively, they could correlate with the late-rift Helmut Shear Zone (Late-Aptian to Early Albian) (Dehler et al., 2016). In any case, the reactivations might have important consequences for hydrothermal vent formations (Magee et al., 2016). The seismic amplitude 3D volume confirmed no evidence of magmatic bodies newer than the Hauterivian volcanic basement.

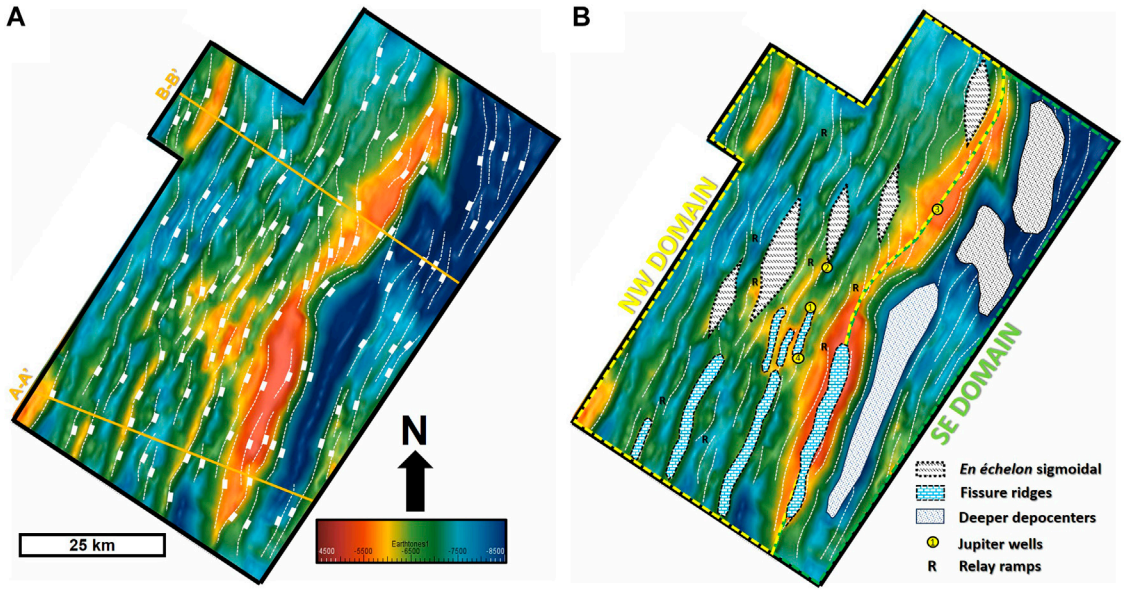

FIGURE 3
(A) Structural map of volcanic basement with syn-rift segmented faults in white dashed lines and dip section locations in orange. **(B)** Structural map of volcanic basement separated by structural domains (yellow and green) with Jupiter wells locations (1)559A, (2)967A, (3)1183, and (4)1246, and examples of the main structural features.

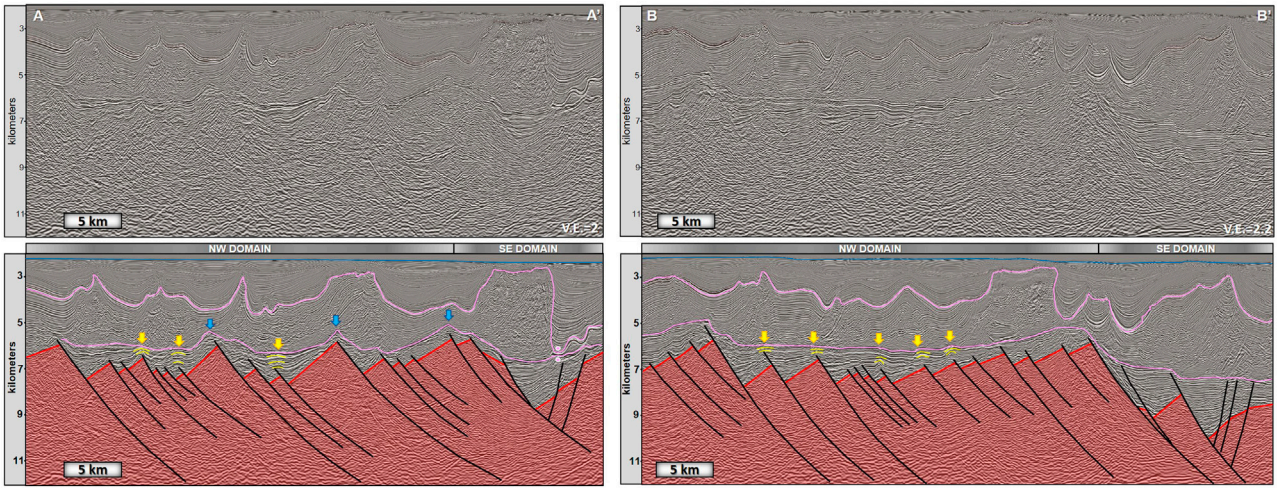

FIGURE 4
Dip sections highlighting volcanic basement hemi-grabens in red color and extensional planar to curved rotational faults in black (domino structural style). Arrows indicate fault-related structures above basement highs: volcanic-like cones and chimneys (yellow) and conical-shaped buildups (blue). V.E.=Vertical Exaggeration. Other horizons: Top and Base of Salt in pink color, Sea Bottom in blue color.

In the Mero Field and in the Iracema/Iara Complex in the Santos Basin, hydrothermal processes, in a low-temperature evaporitic environment, connected to Ca-Mg-Si-rich fluids ascending in subaerial and sublacustrine hydrothermal vents originated the mounds (Souza et al., 2018). Fault activity can influence the development of hydrologically closed lake basins, groundwater flow, and the location of hydrothermal vents, and thermogenic travertine with thermally generated CO_2 of magmatic origin derived from the mantle can classify their deposits (Della Porta, 2015).

The azimuth attribute in the depth slices identified two sets of lineaments: NW-SE and NE-SW (Figure 5), both oblique to the main NNE strike direction of syn-rift faults and clearly crossing over it with *en échelon* patterns in map view. An inflection axis of the syn-rift strike trends from South to North denotes the NE-SW lineaments highlighted in thicker white dashed lines in Figure 5. We interpret this inflection as a direct response to the late-rift left-lateral transtensional Helmut Shear Zone that affected the syn-rift structures (Dehler et al., 2016). The WSW-ENE rift extension axis

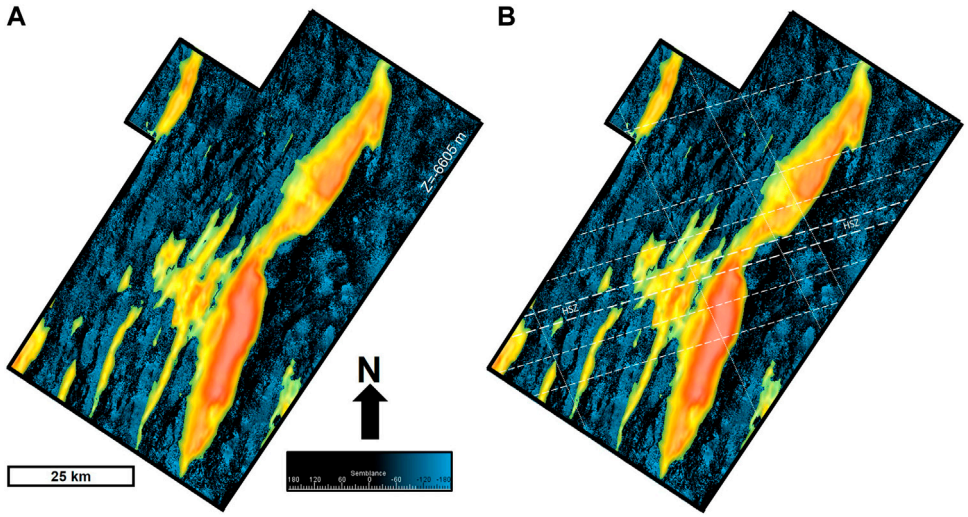

FIGURE 5
Azimuth attribute depth slice at Z = −6605 mm. **(A)** Highlighting the volcanic basement structural highs with same color scale as Figure 3. **(B)** Sets of lineaments interpreted in white dots (NW-SE) and dashed lines (NE-SW). Thicker dashed lines highlight the regional Helmut Shear Zone (HSZ) from Dehler et al. (2016) that caused the inflection of syn-rift structures.

might have originated the syn-rift faults structural styles from strain response, as observed in the East African Rift (Zwaan and Schreurs, 2017) and modeled in the Central Santos Basin (Pereira et al., 2021). The NW-SE lineaments have weaker expression and might relate to the NW-SE rift transfer zones (Meisling et al., 2001).

4.2 Gravimetric potential field

Figures 6–9 present the Bouguer and residual anomalies maps and 2D profiles. We highlighted the location of 2D line 0375 on each map, where we calculated both the Bouguer and residual profiles with the same color scales from the maps. The Bouguer anomaly has both small and large wavelength anomalies (Figures 6, 7). Shallow structures are associated with small wavelength anomalies while deeper structures are associated with larger ones. We interpreted both crustal thinning and Moho oceanward uprising below the Jupiter structure, as the oceanward positive Bouguer gravity gradient in map sight indicates (Figure 6). It corroborates the Moho uprising observed in the wide-angle refraction lines SB01 and SB02 by Evain et al. (2015). The residual anomalies from spectral filtering (Figures 8, 9) show the volcanic basement structural highs and lows (smaller wavelengths). Although the first vertical derivative from the Bouguer gravity anomaly can also correlate with volcanic basement structural highs and lows (Plawiak et al., 2022), this response is usually noisier than residual anomalies from spectral filtering. The Santos Outer High is approximately 300 km in length and the maximum stretching of the crust has approximately 200 km of extension Figures 8, 9. We compared to the refraction lines from Evain et al. (2015): the southeastern part of the Outer High corresponds to Domain A' and the maximum stretching zone represents the extension of Domain B to the northeast (see Evain et al., 2015 for Domains details). We assembled the location of the Continent-Ocean Boundary (COB) by separating high and low frequencies from the map of residual anomalies (Figure 8).

4.3 Seismic amplitude 2D line

Figure 10 shows the wide-angle 2D ultra-deep line 0375 analyzed in this study and the associated gravimetric 2D calculated profiles from Figures 7, 9. We identified amplitude reflectors that may represent the Moho (Figure 10) and we corroborated the crustal thickness variations with interpretations of wide-angle refraction data from Evain et al. (2015). We also observed the oceanward mantle uprising: except for the necking zone with a thickness of approximately 11 km, the crustal thicknesses varies from 28 km at the Hingline to 15 km at the Outer High, decreasing to 5 km at the maximum stretching zone (Figure 10). See Graça et al. (2019) for discussions on crustal thickness of the South Atlantic. We interpreted the COB as a crustal fault and the oceanic crust as being approximately 6 km thick and overlain by volcanic sequences. We also interpreted a gentle mantle uplift under the Jupiter rift shoulder at the edge of the Outer High constrained by Bouguer responses (Figures 7, 10).

Based on the same reflection seismic data set, Zalán et al. (2011) and Kumar et al. (2012) came to divergent conclusions on the crustal architecture of the SSPS. Zalán et al. (2011) interpreted the easternmost part of the SSPS as an exhumed mantle, but we agree with Kumar et al. (2012) who did not find evidence of an exhumed mantle in the line 0375 (Figure 10). Zalán et al. (2011) claimed that a strong continuous reflector, the Conrad discontinuity, separates the crust between a rigid, highly fractured upper part and a ductile lower part. We have not identified any amplitude reflectors related to Conrad within the line 0375 (Figure 10) although a detachment (*décollement*) surface for the syn-rift crustal faults could be inferred as the faults become more horizontal towards this intra-crust surface. Kumar et al. (2012) termed this surface as the "mid-crustal layer".

We interpreted the top volcanic basement and the pre-salt sequences with the syn-rift faults mostly dipping oceanward.

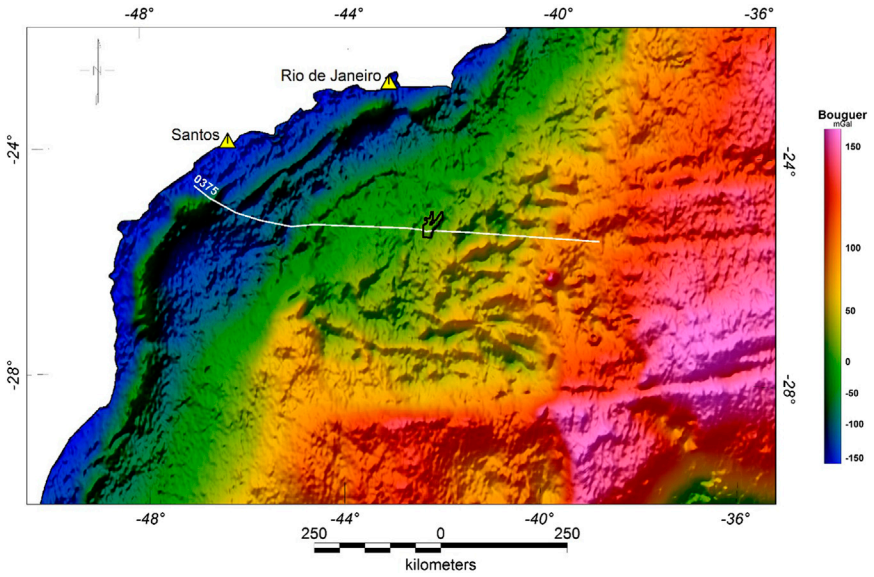

FIGURE 6
Map of Bouguer anomalies obtained from Parker's method (Parker, 1973). 2D seismic line 0375 is indicated in a white line, crossing over the Jupiter prospect in black.

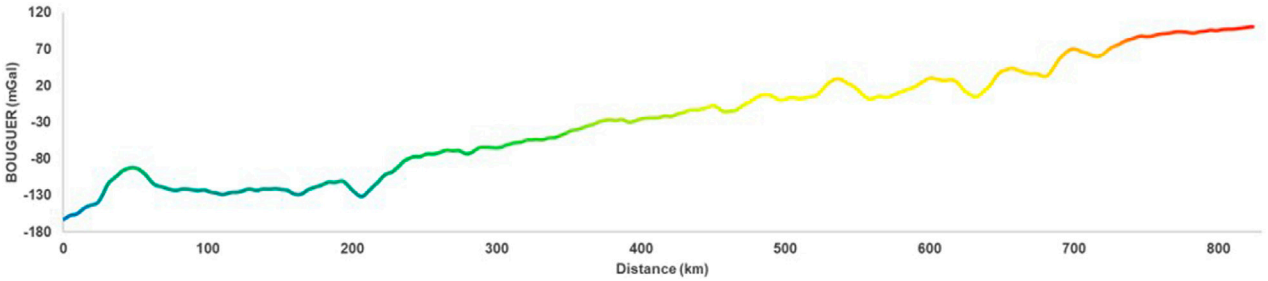

FIGURE 7
Profile of Bouguer anomalies through 2D seismic line 0375. Same color scale as Figure 6.

Deeper fault throws coincide with salt wedges (pink arrows in Figure 10), indicating a long-term deformation caused by deep crustal faulting. Its tectono-structural framework provided the ideal scenario for CO_2 migration through intracrustal faults from the mantle, where degassing may have generated the CO_2. Ros et al. (2017) proposed that a strong lower crust leads to margins characterized by large oceanward dipping faults and strong syn-rift subsidence, and present a COB with an exhumed serpentinized mantle underlain by some magmatic products. Even though we have not interpreted an exhumed mantle in the line 0375, it is interesting to note that the anomalous velocity zone (AVZ) found on the wide-angle refraction SB01 line (Evain et al., 2015) coincides with the maximum stretching zone identified in the line 0357 in this study. Evain et al. (2015) interpreted the AVZ structure as atypical oceanic crust, exhumed lower continental crust, or intruded upper continental crust, overlying either altered mantle in the first two cases or intruded lower continental crust in the last case. See Loureiro et al. (2016) for uncertainty assessment in the wide-angle layered models from Evain et al. (2015). Nevertheless, we have not identified amplitude reflectors that could be associated with igneous bodies. We might expect lower crustal intrusions (magmatic underplating) beneath the SSPS as evidenced in the Faroe-Shetland Basin, NE Atlantic Margin (Layfield et al., 2022).

4.4 Well samples

Both wells cored in Jupiter (3-BRSA-967A-RJS and 3-BRSA-1183-RJS) have representative lithologies of travertine-like carbonates.

They contain wackestones with *in situ* and reworked shrubs and spherulitic grainstone levels that locally vary for micro-conglomerates, silicified breccias, vuggy porosity among the shrubs and fracture zones (Figure 11). Dolomite filaments, pseudo-grainstones, and silicification

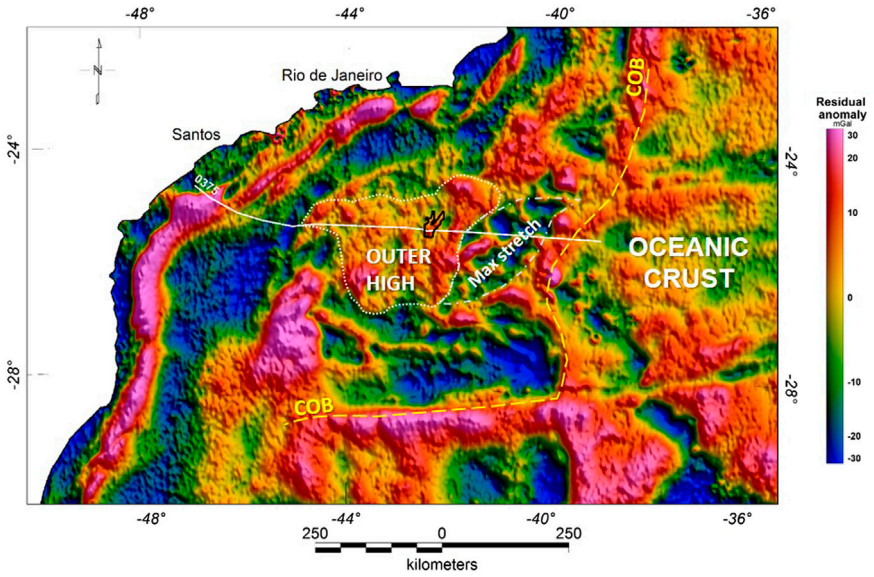

FIGURE 8
Map of residual anomalies obtained from spectral filtering (Nettleton, 1954). 2D seismic line 0375 is indicated in a white line, crossing over the Jupiter prospect in black. Outer High is indicated with the dotted white line and the maximum stretch of the crust in the dashed white line. COB = Continent-Ocean Boundary.

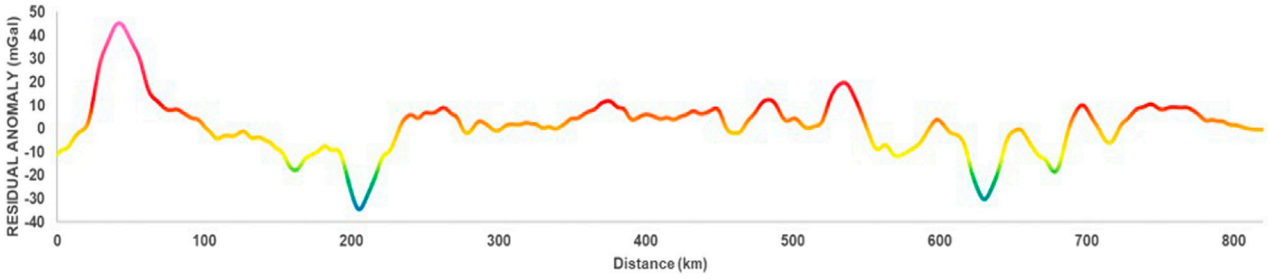

FIGURE 9
Profile of residual anomalies through 2D seismic line 0375. Same color scale as Figure 8.

are present. *In situ* crystal shrubs intercalate with reworked spherulitic calcimudstones/packstones and silica-chert nodules.

The faults and structural highs control mound growth. The facies consist largely of calcite shrubstones and travertine crusts, and thrombolytic facies are absent. These features suggest that ascending hydrothermal brines played an important role in the growth of mounds in the Iara Complex (Sombra et al., 2023). We interpreted similar conclusions from the travertine-like carbonates identified in the Jupiter well cores.

4.5 Well image logging

The image logging results showed a local variability of the maximum horizontal stress orientation around the Jupiter wells (Figure 12). The WSM stress quality rate for the Jupiter wells ranged from A quality (wells 1-BRSA-559A and 3-BRSA-967A) to B quality (wells 3-BRSA-1183 and 3-BRSA-1246). We can use A, B, and C quality stress indicators reliably for analysis of tectonics (Heidbach et al., 2010). The regional Helmut Shear Zone that affected the syn-rift structures (Dehler et al., 2016) possibly influenced the SHmax orientations from wells 559A and 967A, which have SHmax azimuths of 86° and 70° respectively. On the other hand, the syn-rift faults possibly influence the SHmax orientations from the other two wells, 1183 and 1246, which have SHmax azimuths of 28° and 36° respectively.

The present-day maximum horizontal stress orientation is a primary control of fluid flow in the subsurface, both in fractured and unfractured rocks. Large volumes of fluid can flow through active faults and breach hydrocarbon traps (Tingay et al., 2005). The data

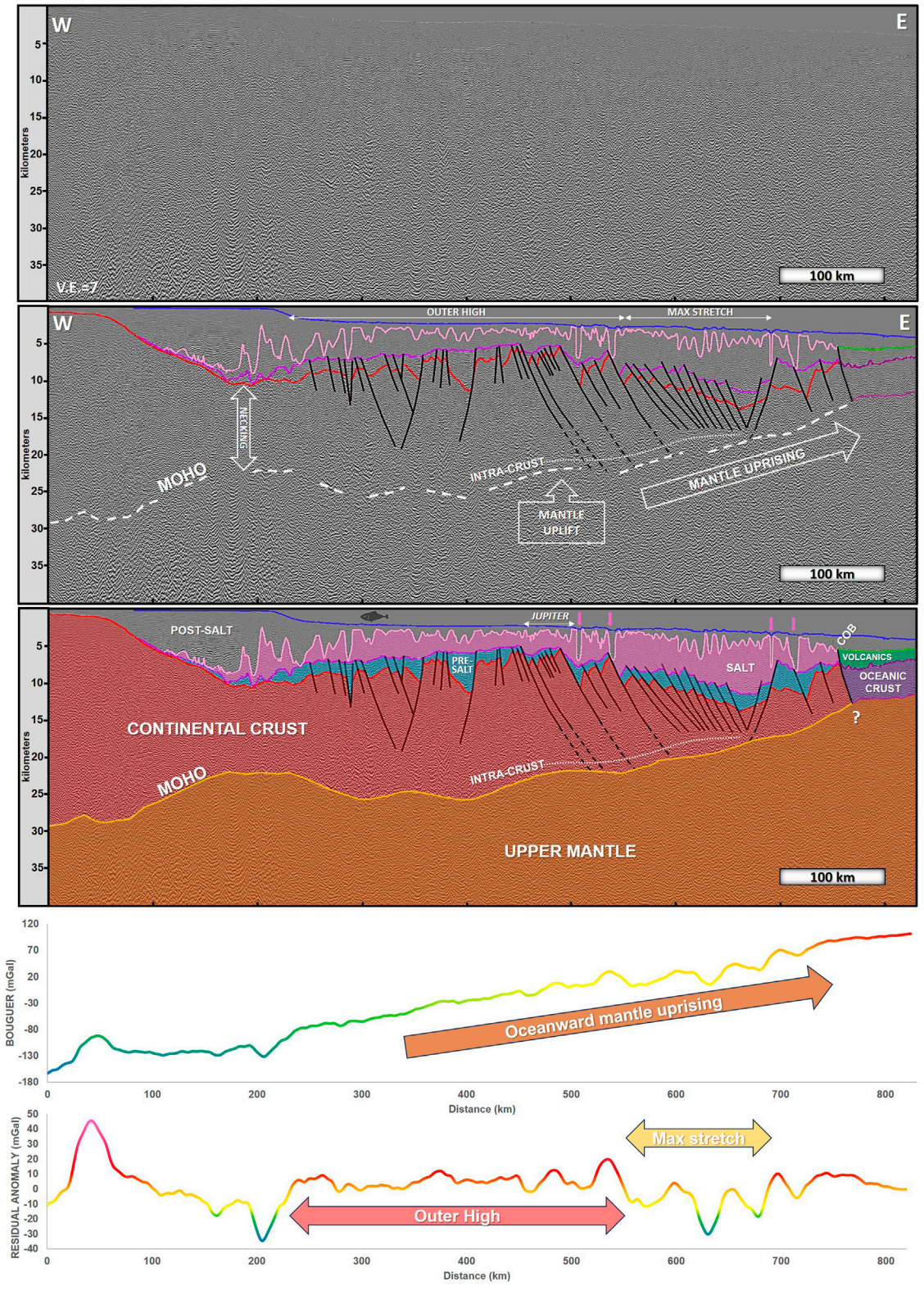

FIGURE 10
2D ultra-deep reflection seismic line 0375 and associated gravimetric profiles. Top: without interpretations. Middle: interpreted with references to main structural features. Bottom: interpreted with references to the main geological features and to the Jupiter structure. COB = Continent-Ocean Boundary. Pink arrows: salt wedges. Horizons: Moho discontinuity (orange), intra-crust inferred detachment (white dotted line), top volcanic basement/continental crust undifferentiated (red), base of salt (dark pink), top of salt (pink), base/top of oceanic crust (purple), offshore volcanics (green), sea bottom (blue). Sequences: pre-salt (light blue), salt (pink), post-salt (no color). Crustal layers: upper mantle (light brown), continental crust (red), oceanic crust (purple), and volcanics (green). Oceanward mantle uprising observed in the profile of Bouguer anomalies (see Figures 7). Delimitation of the Outer High and the maximum stretching zone of the crust observed in the profile of residual anomalies (see Figures 9).

FIGURE 11
Core photograph from well the 3-BRSA-967A-RJS (after Costa et al., 2017), showing representative lithologies of travertine-like carbonates: wackestones containing *in situ* and reworked shrubs and spherulitic grainstone levels locally varying for micro-conglomerates, silicified breccias, vuggy porosity among the shrubs, and fracture zones.

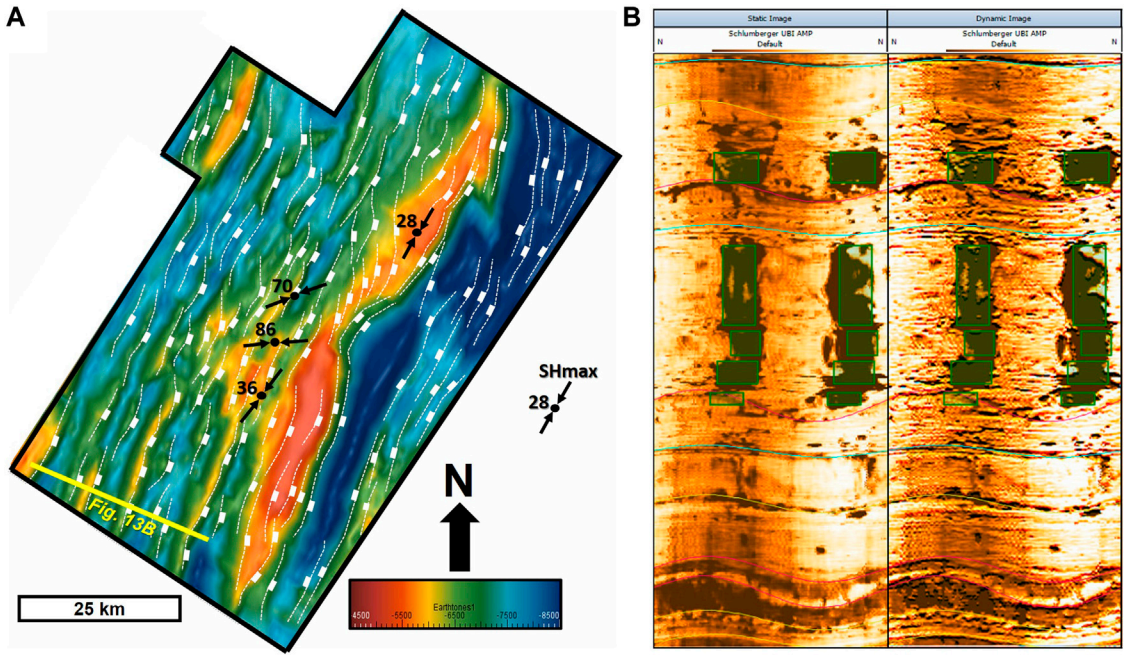

FIGURE 12
(A) Structural map with maximum horizontal stress (SHmax) indications on Jupiter wells. Values represent the SHmax mean azimuths estimated from breakout interpretations. **(B)** An example of static/dynamic acoustic image logging from the well 3-BRSA-1246-RJS, with breakouts in green rectangles.

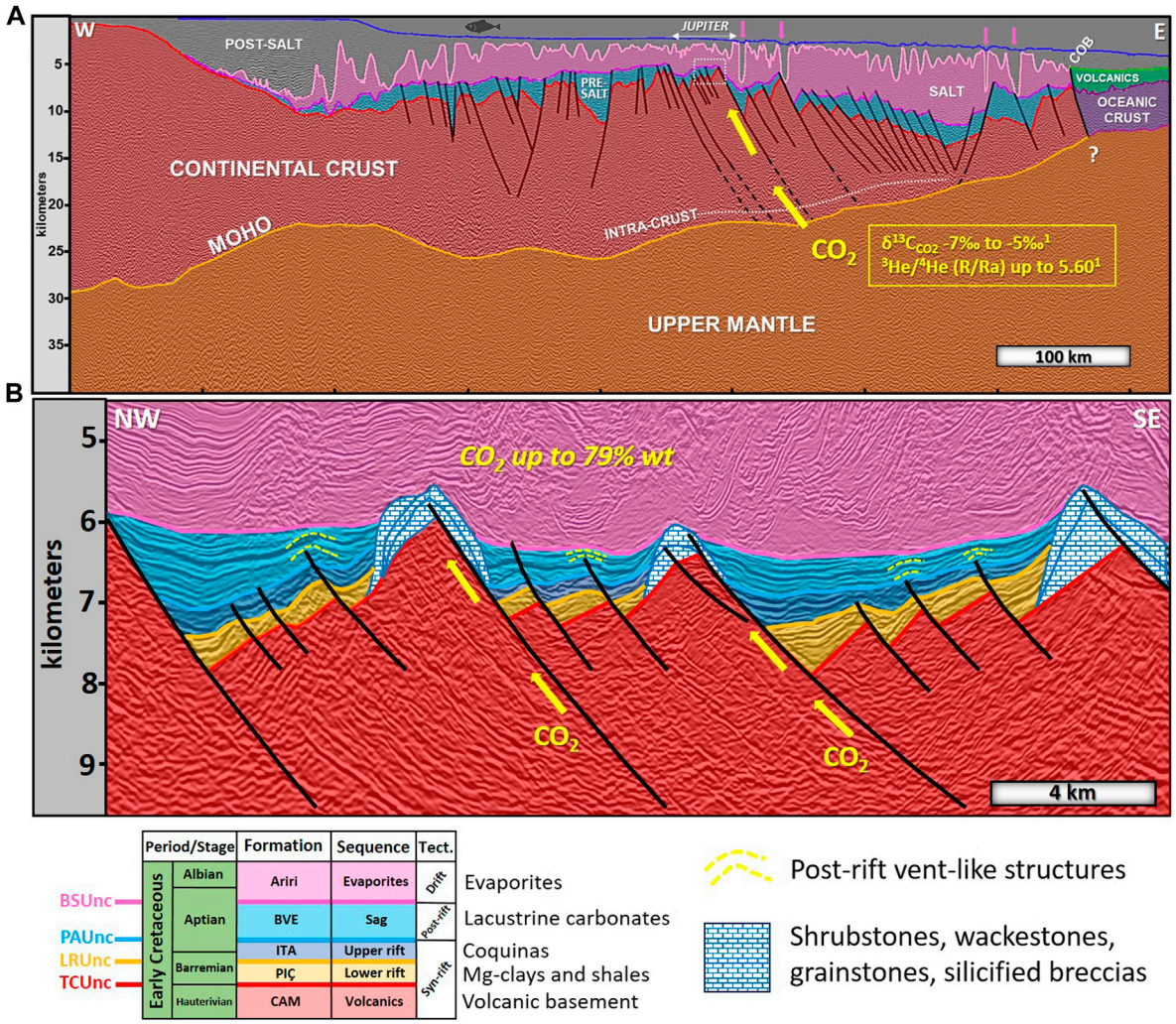

FIGURE 13
Conceptual model of CO2 migration in the Jupiter study area. **(A)** 2D ultra-deep reflection seismic line 0375 showing deep-seated faults acting as pathways for mantle–derived CO_2 indicated by its geochemical mantellic signature. (1) Santos Neto et al. (2012). The white rectangle corresponds to the area of section B. See Figure 10 for color references of geological features. **(B)** dip section on representative structures interpreted in the Jupiter 3D reflection seismic volume showing: lithostratigraphic sequences separated by unconformities (after Moreira et al., 2007); buildups of thermogenic travertines and post-rift vent-like structures. CO_2 % wt represents the maximum value from the Jupiter wells. See Figure 2 for references on unconformities, formations and tectonic events.

did not provide any evidence of active faulting, but the SHmax estimation around the wells might corroborate the influence of regional structures. Moreover, local intersection of structures can form excellent paths for fluid percolation as observed in carbonates in Italy (Billi, 2005). The directions of SHmax observed in the wells might facilitate this percolation: NE-SW for wells 559A and 967A, and NNE for wells 1183 and 1246. However, the paleostress influence might have built up the elongated buildups (fissure ridges).

5 Conclusion

The proposition of a conceptual model for the migration of mantle-derived CO_2 in the Jupiter area, offshore in the Santos Basin (Figure 13), resulted from this analysis. The CO_2 mantle generation and degassing (Santos Neto et al., 2012) and its migration through deep-seated faults in a region of highly stretched continental crust (Ferraz et al., 2019; Gambôa et al., 2019) with oceanward mantle uprising allowed its accumulation in thermogenic travertines (hydrothermal carbonate reservoirs of continental lakes) controlled by basement highs, and its subsequently trapping by evaporites.

Relay ramps and the intersection of structures formed excellent paths for fluid percolation; *in situ* stress (present time) facilitated this percolation according to the directions of SHmax observed in the wells. Silicification and breccias evidenced the hydrothermal percolation through faults, although this conceptual model had not considered the influence of diagenesis.

Conical structures associated with the faults identified on the seismic data may reinforce the hypothesis of active volcanic and/or hydrothermal paleoconduits from the late-rift phase until the

deposition of evaporites. It is most likely related to the late-rift left-lateral transtensional Helmut Shear Zone (Late-Aptian to Early Albian) that affected the syn-rift structures (Dehler et al., 2016), evidenced by: (i) inflection of syn-rift structures; (ii) NE-SW lineaments expression; (iii) *in situ* stress disturbance on the wells 559A and 967A; and (iv) *en échelon* sigmoidal segmentations of syn-rift faults suggesting left-lateral transtensional movement.

The multi-scale approach conceived this conceptual model. A regional 2D seismic line integrated with potential gravimetric field data validated the interpreted crustal structure (Moho discontinuity). Local 3D seismic volume integrated with well data (lithologies and *in situ* stress) helped us to understand the structural framework and its relationship with fluid percolation.

Data availability statement

The datasets presented in this study can be found in online repositories. The name of the repository and accession number can be found below: Exploration and Production Database (BDEP) of the Brazilian Petroleum National Agency—ANP #21855-2.

Author contributions

RP: Conceptualization, Data curation, Formal Analysis, Investigation, Methodology, Software, Supervision, Validation, Visualization, Writing–original draft, Writing–review and editing. MC: Conceptualization, Data curation, Investigation, Methodology, Software, Validation, Writing–review and editing. CS: Data curation, Investigation, Methodology, Visualization, Writing–review and editing. DB: Data curation, Investigation, Software, Visualization. MM: Funding acquisition, Project administration, Resources. AF: Formal Analysis, Funding acquisition, Project administration, Resources, Supervision, Writing–review and editing. LG: Funding acquisition, Resources.

Funding

The author(s) declare financial support was received for the research, authorship, and/or publication of this article.

Acknowledgments

The authors are grateful to Petrogal Brasil S.A. for financial support and publishing permission and to the Brazilian Petroleum National Agency for database and regulation support. We are thankful to the Center for Studies in Biomass and Water Management (NAB) for equipment facilities and to the Fluminense Federal University (UFF)/ Laboratory of Marine Geology (LAGEMAR). With special thanks to the colleagues Dr. André Ettiene Ferraz, Dr. Cleverson Guizan Silva, Dr. Eugênio dos Santos Neto and Dr. Sidney Mello, for fruitful discussions. We are grateful to the Associate Editor Dr. Guillermo Booth-Rea, to the independent reviewers Dr. Simona Todaro and Dr. Laura Gómez de La Peña for constructive and helpful comments, and to Dr. Extor Beason for native English review. All of which have significantly improved the quality and clarity of our manuscript.

Conflict of interest

Author MM was employed by Petrogal Brasil S.A.

The authors declare that this study received funding from Petrogal Brasil S.A. as part of RD&I Project #4370 "Compreendendo as Acumulações de CO_2 na Bacia de Santos/ Platô de São Paulo no Contexto da abertura do Atlântico Sul", under the regulation of the Brazilian Petroleum National Agency—ANP accession number 21855-2. The funder had the following involvement in the study: funding management, research project administration, resources and grant permission for publishing. The funder was not involved in the study design, collection, analysis, interpretation of data, or the writing of this article.

Publisher's note

References

Araujo, M. N., Perez-Gussinye, M., and Mushaldev, I. (2022). Oceanward rift migration during formation of Santos–Benguela ultra-wide rifted margins. *Geol. Soc. Lond. Spec. Pub* 524, 65–91. doi:10.1144/SP524-2021-123

Baptista, R. J., Ferraz, A. E., Sombra, C., Santos Neto, E. V., Plawiak, R., Silva, C. L. L., et al. (2023). The presalt Santos Basin, a super basin of the twenty-first century. *Super. Basin Issue AAPG Bull.* 107 (8), 1369–1389. doi:10.1306/04042322048

Beltrão, R. L. C., Sombra, C. L., Lage, A. C. V. M., Fagundes Netto, J. R., and Henriques, C. C. D. (2009) Challenges and new technologies for the development of the pre-salt cluster, Santos Basin, Brazil, offshore technology conference, OTC-19880. doi:10.4043/OTC-19880-MS

Bigi, S., Beaubien, S. E., Ciotoli, G., D'Ambrogi, C., Doglioni, C., Ferrante, V., et al. (2014). Mantle-derived CO_2 migration along active faults within an extensional basin margin (Fiumicino, Rome, Italy). *Tectonophysics* 637, 137–149. doi:10.1016/j.tecto.2014.10.001

Billi, A. (2005). Attributes and influence on fluid flow of fractures in foreland carbonates of southern Italy. *J. Struct. Geol.* 27, 1630–1643. doi:10.1016/j.jsg.2005.05.001

Carvalho, M., Ferraz, A. E. P. P. D., Ferrari, A. L., Mello, S. L. M., and Gambôa, L. A. P. (2022). Regional-residual separation and enhancement methods applied to regional analysis of potential data: structure of Florianopolis and Rio de Janeiro fracture zones in the western South Atlantic. *Braz. J. Geoph* 40 (2), 1–16. doi:10.22564/brjg.v40i2.2165

Chiodini, G., Cardellini, C., Amato, A., Boschi, E., Caliro, S., Frondini, F., et al. (2004). Carbon dioxide Earth degassing and seismogenesis in central and southern Italy. *Geophys. Res. Lett.* 31, L07615. doi:10.1029/2004GL019480

Cobbold, P. R., Chiossi, D., Green, P. F., Japsen, P., and Bonow, J. (2010). Compressional reactivation, atlantic margin of Brazil: structural styles and consequences for hydrocarbon exploration. Search and Discovery, Article #30114.

Costa, J., Câmara, R., Amthor, J., Storino, V., and Wignall, B. (2017). Relatório de Descrição de Testemunhos Poços 3-RJS-683A-RJS e 3-RJS-713-RJS, Bacia de Santos, Brasil. *Agência Nac. do Petróleo, ANP Internal Report SAA* 13, 17.

Dehler, N. M., Magnavita, L., Gomes, L. C., Rigoti, C. A., Oliveira, J. A. B., Sant'Anna, M. V., et al. (2016). The 'Helmut' geophysical anomaly: a regional left-lateral

transtensional shear zone system connecting Santos and Campos basins, southeastern Brazil. *Mar. Petr. Geol.* 72, 412–422. doi:10.1016/j.marpetgeo.2016.01.012

Della Porta, G. (2015). "Carbonate build-ups in lacustrine, hydrothermal and fluvial settings: comparing depositional geometry, fabric types and geochemical signature," in *Microbial carbonates in Space and time: implications for global exploration and production*. Editors D. W. J. Bosence, K. A. Gibbons, D. P. Le Heron, W. A. Morgan, T. Pritchard, and B. A. Vining (London: Special Pub), 418. Geol. Soc. doi:10.1144/SP418.4

De Luca, P., Carballo, J., Filgueiras, A., Pimentel, G., Esteban, M., Tritlla, J., et al. (2015). "What is the role of volcanic rocks in the Brazilian pre-salt? 77th EAGE conference & exhibition," in IFEMA Conference paper WEN10301. doi:10.3997/2214-4609.201412890

Evain, M., Afilhado, A., Rigoti, C., Loureiro, A., Alves, D., Klingelhoefer, F., et al. (2015). Deep structure of the Santos BasinBasin-São Paulo Plateau System, SE Brazil. *J. Geophys. Res. Solid Earth* 120, 5401–5431. doi:10.1002/2014JB011561

Ferraz, A., Gambôa, L., Santos Neto, E. V., and Baptista, R. (2019). Crustal structure and CO_2 occurrences in the Brazilian basins. *Interpretation* 7, SL37–SL45. doi:10.1190/INT-2019-0038.1

Fetter, M. (2009). The role of basement tectonic reactivation on the structural evolution of Campos Basin, offshore Brazil: evidence from 3D seismic analysis and section restoration. *Mar. Petr. Geol.* 26 (6), 873–886. doi:10.1016/j.marpetgeo.2008.06.005

Freitas, V. A., Vital, J. C. S., Rodrigues, B. R., and Rodrigues, R. (2022). Source rock potential, main depocenters, and CO_2 occurrence in the pre-salt section of Santos Basin. *J. South Am. Earth Sci.*, 115–103760. doi:10.1016/j.jsames.2022.103760

Gambôa, L., Ferraz, A., Baptista, R., and Santos Neto, E. V. (2019). Geotectonic controls on CO_2 formation and distribution processes in the Brazilian pre-salt basins. *Geosciences* 9, 252. doi:10.3390/geosciences9060252

Gomes, P. O., Kilsdonk, B., Minken, J., Grow, T., and Barragan, R. (2009). "The outer high of the Santos Basin, southern São Paulo Plateau, Brazil: pre-salt exploration outbreak, paleogeographic setting, and evolution of the syn-rift structures," in AAPG International Conference and Exhibition. Search and Discovery, Article #10193.

Graça, M. C., Kusznir, N., and Stanton, N. S. G. (2019). Crustal thickness mapping of the central South Atlantic and the geodynamic development of the rio grande rise and walvis ridge. *Mar. Petr. Geol.* 101, 230–242. doi:10.1016/j.marpetgeo.2018.12.011

Heidbach, O., Tingay, M., Bartha, A., Reinecker, J., Kurfess, D., and Müller, B. (2010). Global crustal stress pattern based on the World Stress Map database release 2008. *Tectonophysics* 482 (1-4), 3–15. doi:10.1016/j.tecto.2009.07.023

Heilbron, M., Valeriano, C. G., Tassinari, C. C. G., Almeida, J., Tupinambá, M., Siga, O., Jr., et al. (2008). "Correlation of Neoproterozoic terranes between the Ribeira Belt, SE Brazil and its African counterpart: comparative tectonic evolution and open questions," in *West gondwana: pre-cenozoic correlations across the South Atlantic region*. Editors R. J. Pankhurst, R. A. J. Trouw, B. B. Brito Neves, and M. J. de Wit (London: Special Pub.), 294, 211–237. Geol. Soc. doi:10.1144/SP294.12

Hill, G. J., Wannamaker, P. E., Maris, V., Stodt, J. A., Kordy, M., Unsworth, M. J., et al. (2022). Trans-crustal structural control of CO_2-rich extensional magmatic systems revealed at Mount Erebus Antarctica. *Nat. Commun.* 13, 2989. doi:10.1038/s41467-022-30627-7

Hinze, W. (2003). Bouguer reduction density, why 2.67? *Geophysics* 68 (5), 1559–1560. doi:10.1190/1.1620629

Hutchison, W., Mather, T. A., Pyle, D. M., Biggs, J., and Yirgu, G. (2015). Structural controls on fluid pathways in an active rift system: a case study of the Aluto volcanic complex. *Geosphere* 11 (3), 542–562. doi:10.1130/GES01119.1

Kumar, N., Danforth, A., Nuttall, P., Helwig, J., Bird, D. E., and Venkatraman, S. (2012). From oceanic crust to exhumed mantle: a 40-year (1970–2010) perspective on the nature of crust under the Santos Basin, SE Brazil. *Geol. Soc. Lond. Spec. Publ.* 369 (1), 147–165. doi:10.1144/SP369.16

Kumar, N., and Gambôa, L. A. P. (1979). Evolution of the São Paulo Plateau (southeastern Brazilian margin) and implications for the early history of the South Atlantic. *Geol. Soc. Am. Bull., Part I* 90, 281–293. doi:10.1130/0016-7606(1979)90<281:eotspp>2.0.co;2

Kumar, N., Gambôa, L. A. P., Schreiber, B. C., and Mascle, J. (1977). Geologic history and origin of São Paulo Plateau (southern Brazilian margin), comparison with the Angolan margin, and the early evolution of the northern South Atlantic. *Initial Rep. Deep Sea Drill. Proj. Scripps Institution Oceanogr.* 40, 927–945. doi:10.2973/dsdp.proc.39.140.1977

Layfield, L. K., Schofield, N., Watson, D., Holford, S. P., Jolley, D. W., Kilhams, B. A., et al. (2022). 3D seismic reflection evidence for lower crustal intrusions beneath the faroe–shetland basin, NE atlantic margin. *J. Geol. Soc.* 180. doi:10.1144/jgs2022-172

Lee, H., Kim, H., Kagoshima, T., Park, J. O., Takahata, N., and Sano, Y. (2019). Mantle degassing along strike-slip faults in the Southeastern Korean Peninsula. *Nat. Res.* 9, 15334. doi:10.1038/s41598-019-51719-3

Lee, H., Muirhead, J. D., Fischer, T. P., Ebinger, C. J., Kattenhorn, S. A., Sharp, Z. D., et al. (2016). Massive and prolonged deep carbon emissions associated with continental rifting. *Nat. Geosci.* 9, 145–149. doi:10.1038/NGEO2622

Liu, X., Fu, X., Liu, D., Wei, W., Lu, X., Liu, C., et al. (2018). Distribution of mantle-derived CO_2 gas reservoir and its relationship with basement faults in Songliao Basin, China. *J. Nat. Gas Sci. Eng.* 56, 593–607. doi:10.1016/j.jngse.2018.06.040

Loureiro, A., Afilhado, A., Matias, L., Moulin, M., and Aslanian, D. (2016). Monte Carlo approach to assess the uncertainty of wide-angle layered models: application to the Santos Basin, Brazil. *Tectonophysics* 683, 286–307. doi:10.1016/j.tecto.2016.05.040

Lowenstern, J. B. (2001). Carbon dioxide in magmas and implications for hydrothermal systems. *Miner. Deposita* 36, 490–502. doi:10.1007/s001260100185

Magee, C., Duffy, O. B., Purnell, K., Bell, R. E., Jackson, C. A. L., and Reeve, M. T. (2016). Fault-controlled fluid flow inferred from hydrothermal vents imaged in 3D seismic reflection data, offshore NW Australia. *Basin Res.* 28, 299–318. doi:10.1111/bre.12111

Meisling, K. E., Cobbold, P. R., and Mount, V. S. (2001). Segmentation of an obliquely-rifted margin, campos and Santos basins, southeastern Brazil. *AAPG Bull.* 85 (11), 1903–1924. doi:10.1306/8626d0a9-173b-11d7-8645000102c1865d

Miao, Q., Xu, C., Hao, F., Yin, J., Wang, Q., Xie, M., et al. (2020). Roles of fault structures on the distribution of mantle-derived CO_2 in the Bohai Bay basin, NE China. *J. Asian Earth Sci.* 197, 104398. doi:10.1016/j.jseaes.2020.104398

Moreira, J. L. P., Madeira, C. V., Gil, J. A., and Machado, M. A. P. (2007). Bacia de Santos. *Bol. Geoc. Petrobras.* 15 (2), 531–549.

Nettleton, L. L. (1954). Regionals, residuals, and structures. *Geophysics* 19 (1), 1–22. doi:10.1190/1.1437966

Parker, R. L. (1973). The rapid calculation of potential anomalies. *Geophys. J. Int.* 31 (4), 447–455. doi:10.1111/j.1365-246X.1973.tb06513.x

Pereira, C. E. L., Gomes, C. J. S., and Araújo, M. N. C. (2021). A influência de estruturas preexistentes na formação de riftes oblíquos: o uso da modelagem física e sua comparação com a fase Pré-sal da Bacia de Santos, Brasil. *Braz. Geol. Usp. Sér. Cient.* 21 (4), 103–124. doi:10.11606/issn.2316-9095.v21-181314

Plawiak, R. A. B., Ferraz, A. E. P. P. D., Ferrari, A. L., Mepen, M., and Gambôa, L. A. P. (2022). Seismic scale basement structural mapping in Santos Basin. IX Brazilian symposium of geophysics. Expanded Abstract. 4p.

Rigoti, C. A. (2015). *Tectonic Evolution of Santos Basin with emphasis on crustal geometry: integrated interpretation of seismic reflection and refraction, gravity and magnetic data*. State University of Rio de Janeiro, Master Thesis, 137.

Ros, E., Pérez-Gussinyé, M., Araújo, M., Romeiro, M. T., Andrés-Martínez, M., and Morgan, J. P. (2017). Lower crustal strength controls on melting and serpentinization at magma-poor margins: potential implications for the South Atlantic. *Geochem. Geophys. Geosystems* 18, 4538–4557. doi:10.1002/2017GC007212

Santos Neto, E. V., Cerqueira, J. R., and Prinzhofer, A. (2012). "AAPG annual conv. And exhibition., search and discovery," in *Origin of CO_2 in Brazilian basins*. Article #40969.

Smith, W. H. F., and Wessel, P. (1990). Gridding with continuous curvature splines in tension. *Geophysics* 55 (3), 293–305. doi:10.1190/1.1442837

Sombra, C., Brandão, D., Plawiak, R., Coelho, F., Ferrari, A., and Gambôa, L. (2023). Pre-salt mounds identification: how logs can help. *AAPG Latin America & Caribbean Region and the Brazilian Association of Petroleum Geologists (ABGP), Geosciences Technology Workshop (GTW), oral presentation*. Available at: https://www.aapg.org/global/latinamerica/events/workshop/articleid/64188/the-importance-of-exploration-and-production-in-the-energy-transition#details.

Souza, R. S., Arienti, L. M., Viana, S. M., Falcão, L. C., Cuglieri, M. A., Silva Filho, R. P., et al. (2018). Petrology of the hydrothermal and evaporitic continental cretaceous (Aptian). *Pre-salt Carbonates and Associated Rocks, South Atlantic Santos Basin, Offshore Brazil: AAPG Datapages/Search and Discovery Article #90323*. AAPG Annual Convention and Exhibition. Available at: https://www.searchanddiscovery.com/abstracts/html/2018/ace2018/abstracts/2835691.html.

Tingay, M., Müller, B., Reinecker, J., Heidbach, O., Wenzel, F., and Fleckenstein, P. (2005). Understanding tectonic stress in the oil patch: the world stress map project. *Lead. Edge* 24 (12), 1276–1282. doi:10.1190/1.2149653

Xia, C., Ye, B., Jiang, J., and Hou, Z. (2022). Review of natural origin, distribution, and long-term conservation of CO_2 in sedimentary basins of China. *Earth-Science Rev.* 226, 103953. doi:10.1016/j.earscirev.2022.103953

Yang, J., Qi, N., Ireland, M., Lu, S., Wang, M., Lu, M., et al. (2021). Geological controls on the natural CO_2 accumulation in the surennuoer oilfield of the hailar basin. *China. Mar. Petr. Geol.* 133, 105319. doi:10.1016/j.marpetgeo.2021.105319

Ysaccis, R., El-Toukhy, M., and Moreira, L. M. (2019). *Maximizing the value of seismic data for a better regional understanding and exploration assessment in the Santos Basin, Brazil*. Rio de Janeiro, 5p: Sixteenth International Congress of the Brazilian Geophysical Society.

Zalán, P. V., and Oliveira, J. A. B. (2005). Origem e evolução estrutural do Sistema de Riftes Cenozóicos do Sudeste do Brasil. *Bol. Geoc. Petrobras.* 13 (2), 269–300.

Zalán, P. V., Severino, M. C. G., Rigoti, C. A., Magnavita, L. P., Oliveira, J. A. B., and Vianna, A. R. (2011). An entirely new 3D-view of the crustal and mantle structure of a South Atlantic passive margin-santos, campos and espírito santo basins, Brazil. AAPG annual convention and exhibition, search and discovery article #30177.

Zwaan, F., and Schreurs, G. (2017). How oblique extension and structural inheritance influence rift segment interaction: insights from 4D analog models. *Interpretation* 5 (1), SD119–SD138. doi:10.1190/INT-2016-0063.1